

A study of events with photoelectric emission in the DarkSide-50 liquid argon Time Projection Chamber

P. Agnes^a, I. F. M. Albuquerque^b, T. Alexander^c, A. K. Alton^d, M. Ave^b, H. O. Back^c, G. Batignani^{h,i}, K. Biery^{al}, V. Bocci^x, W. M. Bonivento^j, B. Bottino^{k,l}, S. Bussino^{m,n}, M. Cadeddu^j, M. Cadoni^{o,j}, F. Calaprice^{ae}, A. Caminata^l, N. Canci^p, M. Caravati^j, M. Cariello^l, M. Carlini^{p,q}, M. Carpinelli^{ar,aj}, S. Catalanotti^{s,g}, V. Cataudella^{s,g}, P. Cavalcante^{ap,p}, S. Cavuoti^{s,g,t}, A. Chepurinov^e, C. Cicalò^j, A.G. Cocco^g, G. Covone^{s,g}, D. D'Angelo^{ao,v}, S. Davini^l, A. De Candia^{s,g}, S. De Cecco^{x,y}, G. De Filippis^{s,g}, G. De Rosa^{s,g}, A. V. Derbin^z, A. Devoto^{o,j}, M. D'Incecco^p, C. Dionisi^{x,y}, F. Dordei^j, M. Downing^{ab}, D. D'Urso^{ar,aj}, G. Fiorillo^{s,g}, D. Franco^{ad}, F. Gabriele^j, C. Galbiati^{ae,p,q}, C. Ghiano^p, C. Giganti^w, G. K. Giovanetti^{ae}, O. Gorchakov^{ah,1}, A.M. Goretti^p, A. Grobov^{aa,ag}, M. Gromov^{e,ah}, M. Guan^{ai}, Y. Guardincerri^{al,1}, M. Gulino^{1,aj}, B. R. Hackett^c, K. Herner^{al}, B. Hosseini^j, F. Hubaut^f, E.V. Hungerford^a, An. Ianni^{ae,p}, V. Ippolito^x, K. Keeter^{as}, C. L. Kendziora^{al}, I. Kochanek^p, D. Korablev^{ah}, G. Korga^{a,p}, A. Kubankin^{an}, M. Kuss^h, M. La Commara^{s,g}, M. Lai^{o,j}, X. Li^{ae}, M. Lissia^j, G. Longo^{s,g}, I. N. Machulin^{aa,ag}, L. P. Mapelli^{aq}, S. M. Mari^{m,n}, J. Maricic^{af}, C. J. Martoff^{am}, A. Messina^{x,y}, P. D. Meyers^{ae}, R. Milincic^{af}, M. Morrocchi^{h,i}, V. N. Muratova^z, P. Musico^l, A. Navrer Agasson^w, A.O. Nozdrina^{aa,ag}, A. Oleinik^{an}, F. Ortica^{at,au}, L. Pagani^{ac}, M. Pallavicini^{k,l}, L. Pandola^{aj}, E. Pantic^{ac}, E. Paoloni^{h,i}, K. Pelczar^{p,u}, N. Pelliccia^{at,au}, E. Picciau^{o,j}, A. Pocar^{ab}, S. Pordes^{al}, S. S. Poudel^a, P. Pralavorio^f, F. Ragusa^{ao,v}, M. Razeti^j, A. Razeto^p, A. L. Renshaw^a, M. Rescigno^x, J. Rode^{p,w}, A. Romani^{at,au}, D. Sablone^{ae,p}, O. Samoylov^{ah}, W. Sands^{ae}, S. Sanfilippo^{n,m}, C. Savarese^{q,p,ae}, B. Schlitzer^{ac}, D. A. Semenov^z, A. Shchagin^{an}, A. Sheshukov^{ah}, M. D. Skorokhvatov^{aa,ag}, O. Smirnov^{ah}, A. Sotnikov^{ah}, S. Stracka^h, Y. Suvorov^{s,g,aa}, R. Tartaglia^p, G. Testera^l, A. Tonazzo^{ad}, E. V. Unzhakov^z, A. Vishneva^{ah}, R. B. Vogelaar^{ap}, M. Wada^{ae,j,ak}, H. Wang^{aq}, Y. Wang^{aq,ai}, S. Westerdale^{ae,j}, Ma. M. Wojcik^u, X. Xiao^{aq}, C. Yang^{ai}, G. Zuzel^u

^a*Department of Physics, University of Houston, Houston, TX 77204, USA*

^b*Instituto de Física, Universidade de São Paulo, São Paulo 05508-090, Brazil*

^c*Pacific Northwest National Laboratory, Richland, WA 99352, USA*

^d*Physics Department, Augustana University, Sioux Falls, SD 57197, USA*

^e*Skobeltsyn Institute of Nuclear Physics, Lomonosov Moscow State University, Moscow 119234, Russia*

^f*Centre de Physique des Particules de Marseille, Aix Marseille Univ, CNRS/IN2P3, CPPM, Marseille, France*

^g*INFN Napoli, Napoli 80126, Italy*

^h*INFN Pisa, Pisa 56127, Italy*

ⁱ*Physics Department, Università degli Studi di Pisa, Pisa 56127, Italy*

^j*INFN Cagliari, Cagliari 09042, Italy*

^k*Physics Department, Università degli Studi di Genova, Genova 16146, Italy*

^l*INFN Genova, Genova 16146, Italy*

^m*INFN Roma Tre, Roma 00146, Italy*

ⁿ*Mathematics and Physics Department, Università degli Studi Roma Tre, Roma 00146, Italy*

¹Deceased.

- ^o*Physics Department, Università degli Studi di Cagliari, Cagliari 09042, Italy*
^p*INFN Laboratori Nazionali del Gran Sasso, Assergi (AQ) 67100, Italy*
^q*Gran Sasso Science Institute, L'Aquila 67100, Italy*
^r*Museo della fisica e Centro studi e Ricerche Enrico Fermi, Roma 00184, Italy*
^s*Physics Department, Università degli Studi "Federico II" di Napoli, Napoli 80126, Italy*
^t*INAF Osservatorio Astronomico di Capodimonte, 80131 Napoli, Italy*
^u*M. Smoluchowski Institute of Physics, Jagiellonian University, 30-348 Krakow, Poland*
^v*INFN Milano, Milano 20133, Italy*
^w*LPNHE, CNRS/IN2P3, Sorbonne Université, Université Paris Diderot, Paris 75252, France*
^x*INFN Sezione di Roma, Roma 00185, Italy*
^y*Physics Department, Sapienza Università di Roma, Roma 00185, Italy*
^z*Saint Petersburg Nuclear Physics Institute, Gatchina 188350, Russia*
^{aa}*National Research Centre Kurchatov Institute, Moscow 123182, Russia*
^{ab}*Amherst Center for Fundamental Interactions and Physics Department, University of Massachusetts, Amherst, MA 01003, USA*
^{ac}*Department of Physics, University of California, Davis, CA 95616, USA*
^{ad}*APC, Université de Paris, CNRS, Astroparticule et Cosmologie, Paris F-75013, France*
^{ae}*Physics Department, Princeton University, Princeton, NJ 08544, USA*
^{af}*Department of Physics and Astronomy, University of Hawai'i, Honolulu, HI 96822, USA*
^{ag}*National Research Nuclear University MEPhI, Moscow 115409, Russia*
^{ah}*Joint Institute for Nuclear Research, Dubna 141980, Russia*
^{ai}*Institute of High Energy Physics, Beijing 100049, China*
^{aj}*INFN Laboratori Nazionali del Sud, Catania 95123, Italy*
^{ak}*AstroCeNT, Nicolaus Copernicus Astronomical Center, 00-614 Warsaw, Poland*
^{al}*Fermi National Accelerator Laboratory, Batavia, IL 60510, USA*
^{am}*Physics Department, Temple University, Philadelphia, PA 19122, USA*
^{an}*Radiation Physics Laboratory, Belgorod National Research University, Belgorod 308007, Russia*
^{ao}*Physics Department, Università degli Studi di Milano, Milano 20133, Italy*
^{ap}*Virginia Tech, Blacksburg, VA 24061, USA*
^{aq}*Physics and Astronomy Department, University of California, Los Angeles, CA 90095, USA*
^{ar}*Chemistry and Pharmacy Department, Università degli Studi di Sassari, Sassari 07100, Italy*
^{as}*School of Natural Sciences, Black Hills State University, Spearfish, SD 57799, USA*
^{at}*INFN Perugia, Perugia 06123, Italy*
^{au}*Chemistry, Biology and Biotechnology Department, Università degli Studi di Perugia, Perugia 06123, Italy*

Abstract

Finding unambiguous evidence of dark matter interactions in a particle detector is a main objective of physics research. The liquid argon time projection chamber technique for the detection of Weakly Interacting Massive Particles (WIMP) allows sensitivities down to the so-called neutrino floor for high and low WIMP masses. Based on the successful operation of the DarkSide-50 detector, a new and more sensitive experiment, DarkSide-20k, was designed and is now under construction. A thorough understanding of the DarkSide-50 detector response to events classified as dark matter as well as all other interactions is essential for an optimal design of the new experiment. In this paper, we report on a particular set of events, for which scintillation-ionization signals are observed in association with signals from single or few isolated electrons. We identified and provided an interpretation for two event types in which electrons are produced via photoelectric effect on the cathode electrode and

in the bulk liquid. Events with photoelectric emissions are observed in association with most interactions with large energy depositions in the detector. From the measured rate of these events, we determine the photo-ionization probability, or photoelectric quantum efficiency, of tetraphenyl butadiene (TPB) at wavelengths around 128 nm.

Keywords: Dark matter, liquid argon, underground argon

1. Introduction

Direct detection of Weakly Interacting Massive Particle Dark Matter (WIMP DM) is one of the most active areas of astroparticle physics. The Liquid Argon (LAr) Time Projection Chamber (TPC) technology offers a path to reach sensitivities down to the so-called neutrino floor, for both high and low WIMP masses. Based on the successful operation of the DarkSide-50 (DS-50) detector [1, 2], a new and more sensitive experiment, DarkSide-20k [3], has been designed and is now under construction. A thorough understanding of the detector response of DS-50 is therefore key to optimizing the new experiment. To this end, it is important to scrutinize all event types occurring in the detector alongside those classified as dark matter candidates.

A typical interaction in the active volume of the TPC yields a prompt scintillation signal, S1, and one or more clouds of ionization electrons, depending on the single- or multi-scatter nature of the interaction. In the DS-50 LAr TPC, ionization electrons drift upwards under a uniform electric field and are, via appropriately applied electric fields, extracted into a thin layer of argon gas where they induce one or more electroluminescence signals, S2. As discussed in [4], S1 and S2 signals have different pulse shapes. The S1 signal has a fast rise-time of a few ns and falls as a double exponential, with $\tau_1 = (6 \pm 1)$ ns and $\tau_2 = (1.5 \pm 0.1)$ μ s. The amplitude ratio between the two decay components is ~ 3 for nuclear recoils and ~ 0.3 for electron recoils [5, 6]. This differ-

ence leads to a very effective Pulse Shape Discrimination (PSD) between electron and nuclear recoils. The S2 signal has a ~ 1 μ s rise-time and a ~ 3 μ s fall-time. Detecting both the S1 and S2 pulses of each event allows three-dimensional reconstruction of the interaction position and, in turn, background rejection by requiring localized energy depositions and by volume fiducialization.

In this paper, we study a particular class of events with small-amplitude pulses appearing in the same 440 μ s acquisition window of normal S1-S2 events. These events are selected with distinctive features that clearly separate them from multi-scatter interactions with two S2 pulses. We require one of the S2 pulses to either have a specific time correlation with the S1 or S2 signals or to be consistent with it originating from one single drifting electron, or both. We also provide a preliminary interpretation of the observed event types. More studies, perhaps with other detectors, are needed for a complete picture. A sub-set of these events was already presented in a previous DS-50 paper [7]. Single electron signals were also studied in liquid xenon detectors [8, 9, 10, 11, 12, 13, 14, 15, 16].

2. The DarkSide-50 detector

The DS-50 LAr TPC detects light from both S1 and S2 using 38 3" photomultipliers (PMTs) arranged in two arrays of 19 PMTs each, at both ends of the (46.4 ± 0.7) kg cylindrical active target of low-radioactivity underground argon

(UAr) [7, 17, 18]. The PMTs are submerged in liquid argon and view the active volume through fused silica windows. These are coated on both faces with transparent conductive indium tin oxide (ITO) films 15 nm thick. The inner window faces define the grounded anode (top) and HV cathode (bottom) of the TPC, while the outer faces are kept at the average photocathode potential of each 19-PMTs array. The cylindrical side wall is made of 2.54 cm-thick polytetrafluoroethylene (PTFE) reflector sintered using a special annealing cycle to increase its reflectivity. The PTFE reflector and the fused silica windows are coated with tetraphenyl butadiene (TPB) wavelength shifter, which absorbs the 128 nm LAr scintillation photons and re-emits visible photons with a peak wavelength of 420 nm. The thickness of the TPB coating on the windows varies between $(230 \pm 10) \mu\text{g}/\text{cm}^2$ at the center and $(190 \pm 15) \mu\text{g}/\text{cm}^2$ at the edge of the active volume. The thickness of the TPB on the cylindrical wall is $(165 \pm 20) \mu\text{g}/\text{cm}^2$ at half-height and $(224 \pm 27) \mu\text{g}/\text{cm}^2$ at the top and bottom. The electric fields needed for drifting and extracting electrons consists of the ITO-coated cathode and anode planes, a field cage comprising a stack of copper rings behind the PTFE reflector held at graded potentials, and a grid that separates the drift and electron extraction regions. The grid, placed 5 mm below the liquid surface, is a hexagonal mesh photo-etched from a 50 μm -thick stainless steel foil and has an optical transparency of 95% at normal incidence.

The data reported here were acquired between July 2015 and October 2017, using a TPC drift field of 200 V/cm, an extraction field of 2.8 kV/cm, and an electroluminescence field of 4.2 kV/cm. At this extraction field, the efficiency for extracting ionization electrons into the gas layer is estimated to be $>99.9\%$ [19]. The electron drift time,

i.e., the time difference $\Delta t_{\text{S2-S1}}$ between the S2 and S1 signals, has its maximum value at $t_{\text{drift}}^{\text{max}} = 376 \mu\text{s}$ for events located at the cathode. The electron drift speed at this field is $(0.93 \pm 0.01) \text{ mm}/\mu\text{s}$ [20].

A hardware event trigger in DS-50 occurs when 2 or more PMT signals exceed a threshold of 0.6 Photo-Electrons (PE) within a 100 ns window [20]. Waveform data are recorded from all 38 PMTs for 440 μs starting $\sim 10 \mu\text{s}$ before the trigger. Subsequent triggers are inhibited for 800 μs . Software pulse-finding algorithms are then applied to the digitized data, including the pre-trigger data. The software classifies pulses in two categories (S1 or S2) based on the fraction of light detected within the first 90 ns (f_{90}). The efficiency of the software pulse-finding algorithm is essentially 100% for S2 signals larger than 30 PE [21]. The pulse finder uses an integration window of 30 μs , which is long enough to include the entire S2 signal.

The argon is continuously purified by recirculating it in gaseous form through a heated getter (SAES Monotorr PS4-MT50-R-2), which reduces contaminants such as O_2 and N_2 to sub-ppb levels, and through a cold charcoal radon trap. The measured electron drift lifetime was larger than $\sim 10 \text{ ms}$ during the whole data-taking, indicating $\sim 30 \text{ ppt}$ O_2 -equivalent contamination [22].

3. Event selection

We select three-pulse events, triggered by an S1 signal followed by two S2 signals. One of these S2-like pulses is required to have a charge $< 200 \text{ PE}$, and is labeled as a Single Electron Candidate (SEC).

We require that the event trigger occurs at least 400 μs after the end of the inhibit window of the previous trigger (it *i.e.*, at least 1.21 ms after the previous trigger).

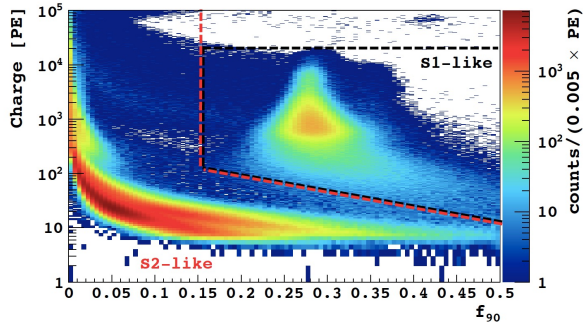


Figure 1: Pulse charge in photoelectrons, PE, *vs.* pulse shape discrimination parameter, f_{90} , for all pulses in events with three pulses. The S1-like pulse selection corresponds to the area to the right of the the black dashed line, while the S2-like pulse selection corresponds to the area to the left of the red dashed line.

This removes events that triggered on an S2 whose S1 occurred during the inhibit window [7]. Since the detector response of DS-50 displays a strong radial dependence of the S2 light yield [1], we only select events for which the central top PMT records the most light for SEC candidate pulses to avoid dealing with sizeable efficiency corrections. As discussed in a previous DS-50 paper [1], the mean S2 signal from single electrons when the maximum signal is in the central top PMT is 23 ± 1 PE. Figure 1 shows the S1 *vs.* S2 identification in events with three pulses by appropriate selections in the pulse charge *vs.* pulse shape discrimination parameter (f_{90}) distribution. We restrict our selection to electron-recoil events by requiring $f_{90} < 0.5$.

We classify the selected events in two groups, according to the time sequence of the three pulses: S1-S2-SEC, with the SEC occurring after the S2 signal, and S1-SEC-S2, with the SEC occurring between S1 and S2.

To further strengthen the correct identification of the pulse sequence, we require the ratio of S2 to S1 to be >10 , as expected when the two pulses come from the same interaction. Indeed, in DS-50, the typical

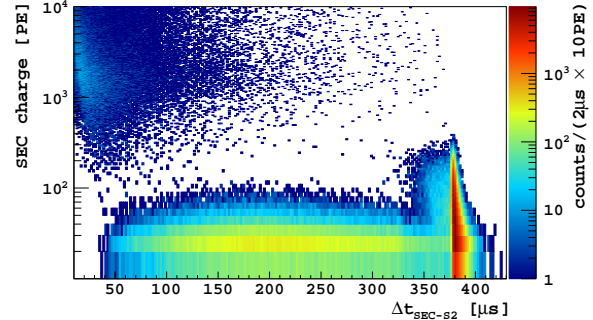


Figure 2: SEC charge *vs.* time difference between the SEC and the preceding S2 pulse, $\Delta t_{\text{SEC-S2}}$. The population at small values of $\Delta t_{\text{SEC-S2}}$ and large values of charge is related to double-scatter γ -ray interactions.

S2 to S1 charge ratio is between ten and thirty.

4. Events with photoelectric effect on the cathode

For S1-S2-SEC events, Fig. 2 shows the charge of the SEC pulse *vs.* the time difference between the SEC and the preceding S2 ($\Delta t_{\text{SEC-S2}}$). We observe three main populations of SECs depending on how late they occur after the S2 pulse and on the SEC charge amplitude.

One population of events corresponds to $\Delta t_{\text{SEC-S2}} \sim 380 \mu\text{s}$, with SEC charge peaking at about 25 PE but extending up to a couple 100 PEs. The time difference $\Delta t_{\text{SEC-S2}}$ is compatible with the maximum drift time $t_{\text{drift}}^{\text{max}}$. Therefore, it is plausible to assume that these events correspond to photoelectric extractions from the cathode by S2 photons. We call these events *S2-echoes*. The number of detected S2-echo events is affected by the limited data acquisition time window, $430 \mu\text{s}$ after the trigger. This time window is $< 2t_{\text{drift}}^{\text{max}}$, the time required to include all S2-echoes. Specifically, for an interaction occurring in proximity of the cathode, $\sim t_{\text{drift}}^{\text{max}}$ is needed for the S2 signal and another $t_{\text{drift}}^{\text{max}}$ for the S2-echo. The DS-50 data acquisition only recorded

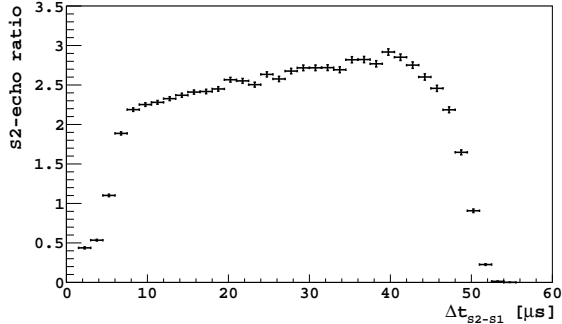


Figure 3: Ratio between events containing an S2-echo and standard S1-S2 events, as a function of the drift time, Δt_{S2-S1} .

S2-echo events originating from primary interactions in the top section of the TPC, with drift times $\leq (430 \mu\text{s} - t_{\text{drift}}^{\text{max}})$. This is illustrated in Fig. 3, which shows the ratio between events containing an S2-echo and standard S1-S2 events, as a function of their drift time (the normalisation accounts for the different background rates along the chamber drift axis). The cutoff above $\sim 50 \mu\text{s}$ reflects the limited data-acquisition time window. The drop below $\sim 10 \mu\text{s}$ is due to the inefficiency of the pulse-finder algorithm in reconstructing two pulses which are too close in time. This effect is also observed in normal S1-S2 events.

Another event population in Fig. 2 has $\Delta t_{\text{SEC-S2}}$ between $50 \mu\text{s}$ and $375 \mu\text{s}$ and SEC charges up to ~ 80 PE, peaking at ~ 25 PE, the single-electron response. These events are well separated from the event population at SEC charges larger than a few 100 PEs, that are instead identified as S2 events from standard double-scatter γ -ray interactions in the detector. The nature of the low SEC charge events is clearly emerging from Fig. 4, which shows the distribution of $\Delta t_{\text{SEC-S2}}$ vs. $\Delta t_{\text{SEC-S1}}$ where, to highlight the behavior of small charge signals, we apply the cut $\text{SEC} < 50$ PE. A vertical band corresponding to $\Delta t_{\text{SEC-S1}} \sim 380 \mu\text{s}$ is clearly emerging in this distribution, ex-

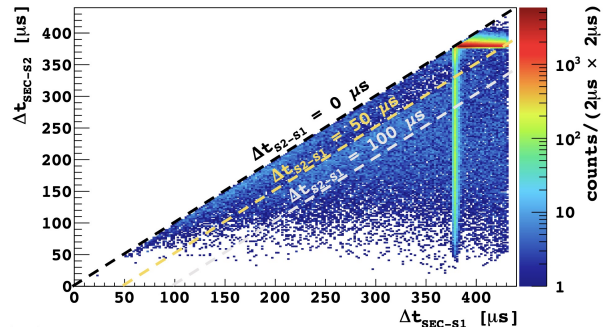


Figure 4: Time difference $\Delta t_{\text{SEC-S2}}$ vs. time difference $\Delta t_{\text{SEC-S1}}$ distribution for events with $\text{SEC} < 50$ PE. Lines corresponding to constant Δt_{S2-S1} values are also shown.

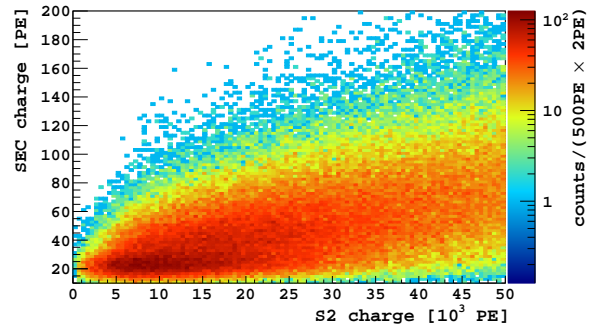


Figure 5: SEC charge vs. S2 charge distribution for S2-echo events.

actly one maximum drift time after the S1 signal. We identify these events as photoelectric extractions from the cathode by S1 photons and call them *S1-echoes*.

To further test our interpretation of S2-echo events as S2-induced photoelectric extractions at the cathode, we investigated the correlation between SEC and S2 charges. The expectation is that the larger the S2 charge, the higher the photon flux hitting the cathode and the corresponding number of extracted electrons. Such a correlation is visible in Figure 5, supporting this hypothesis.

The fraction, F , of selected two and three-pulse events in the various categories, with the cut $10 \mu\text{s} < \Delta t_{S2-S1} < 50 \mu\text{s}$ applied to have uniform S2-echo events selection probability for all drift times is shown in Tab. 1.

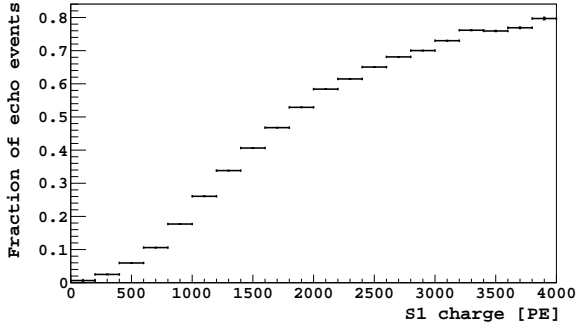


Figure 6: Fraction of events containing echoes *vs.* S1 charge, with $\Delta t_{S2-S1} < 50\mu s$.

The table also includes the fraction of standard S1-S2 events and of S-liquid events, which will be discussed in Sec. 5. In order to keep a proper normalisation with the echo events, the number of standard S1-S2 events is divided by the number of PMTs in the top array. It can be noticed that the fraction of events with an S-echo is $>65\%$, with $\sim 2.5\%$ of them S1-echoes.

We also expect larger pulses to have larger probability to produce echoes. We, therefore, studied the fraction of events with an echo as a function of the S1 charge, as shown for $\Delta t_{S2-S1} < 50\mu s$ in Fig. 6. This fraction is found to monotonically increase with the S1 charge, supporting our hypothesis. Indeed, echoes occur in more than 80% of the interactions at the higher energy range considered.

From the fraction of S1-echo events it is possible to measure the photoelectric emission probability from the cathode, P_{ph} , at the liquid argon emission wavelengths around 128 nm. For this calculation, we remove the restriction in the event selection of three hits in the event. This criterion is applied to avoid the need of efficiency corrections in the calculation of the photoelectric emission probability from the cathode. P_{ph} is derived as:

$$P_{ph} = \langle R_{S1-echo} \rangle \times \frac{g_1}{\langle S1 \rangle \cdot \epsilon_{geo}}, \quad (1)$$

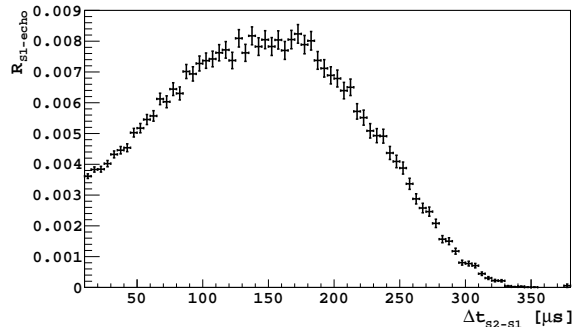


Figure 7: Fraction of events with an S1-echo *vs.* drift time Δt_{S2-S1} .

with $\langle R_{S1-echo} \rangle = (6.4 \pm 0.1) \times 10^{-3}$ the average S1-echo fraction, referred to Fig. 7, $\langle S1 \rangle = (1318 \pm 1)$ PE the average S1 charge, and $g_1 = (0.157 \pm 0.001)$ PE/photon [23]. The optical geometric acceptance ϵ_{geo} was determined assuming that the S1 photon hits the cathode in the area corresponding to the central PMT, and we found $\epsilon_{geo} = (8.6 \pm 1.3) \times 10^{-3}$. The dominant uncertainty on this quantity comes from neglecting the number of photons hitting the cathode in an area between PMTs and was evaluated comparing the cathode surface covered by PMTs with the total area and dividing it by the number of the top array PMTs. Combining all uncertainties, we obtain $P_{ph} = (0.9 \pm 0.2) \times 10^{-4}$.

Since the measured absorption length at 128 nm is about 400 nm [24], much less than the few μm thickness of the TPB on the cathode (see Sec. 2), most of the photons are expected to interact in the TPB. P_{ph} is thus a good measurement of the photoelectric quantum efficiency of TPB, unmeasured so far.

The dependence of the fraction of S1-echo events on drift time is shown in Fig. 7, obtained without the requirement of three pulses in the event. From the qualitative point of view, this different selection has a marginal effect on the behavior of distribution. We observe a rise in the event number up to about 150 μs , as expected from ge-

Table 1: Fraction (F) of selected events in two and three-pulse events in the various categories: S1-S2 are regular two pulse events with a scintillation and an ionization pulse, S-echo signals include both S1-echo and S2-echo pulses due to electron extraction from the cathode, and S-liquid signals represent S1 and S2 signals due to electron extraction from the liquid, as discussed in Sec. 5. The selection $10\mu s < \Delta t_{S2-S1} < 50\mu s$ was applied. The number of standard S1-S2 events is divided by the number of PMTs in the top array. The denominator is defined as the sum of all categories with $SEC < 200$ PE. The S-echo signals are discussed in Sec. 4, while S-liquid signals in Sec. 5. For the S1-echo selection, it is also required that the event is not an S2-echo.

<i>Category</i>	Δt <i>cut</i>	<i>SEC cut</i>	F (%)
S1-S2	-	-	25.6 ± 0.1
S-echo signals	-	< 200 PE	65.6 ± 0.1
S2-echo	$375\mu s < \Delta t_{SEC-S2} < 385\mu s$	< 200 PE	63.9 ± 0.1
S1-echo	$375\mu s < \Delta t_{SEC-S1} < 385\mu s$	< 200 PE	1.69 ± 0.03
S-liquid signals	-	< 50 PE	8.00 ± 0.05
S2-liquid	$\Delta t_{SEC-S2} > 0$ & not-echo	< 50 PE	7.96 ± 0.06
S1-liquid	$\Delta t_{SEC-S2} < 0$ & not-echo	< 50 PE	0.037 ± 0.005

ometric acceptance effects but, contrary to the expectations, we observe a decrease at large drift times. This effect is explained by the different energy distribution of background events in the top part of the TPC compared to the bottom, possibly due to the asymmetry in material distribution and, therefore, in the radioactivity load. Interestingly, we observe an almost three-fold difference of the mean S1 energy of S1-echo events for small and large drift times.

5. Events with photoelectric effect in the liquid

In addition to events with photoelectric effect on the cathode (S-echo signals), we also observe in Fig. 4 events with time differences unrelated to cathode emission. We assume that these events are due to photoelectric extraction on some species in the liquid, such as meta-stable argon anions or trace contaminants. We call these events *S2-liquid*, since with the time sequence S1-S2-SEC, the SECs with single electron charge are predominantly induced by S2 photons. It is also possible to observe a similar kind of phenomenology by studying events with the

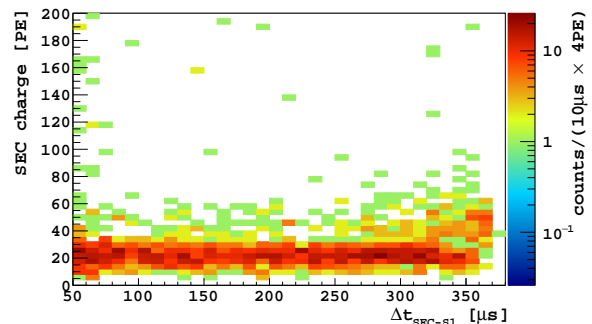


Figure 8: SEC charge *vs.* time difference Δt_{SEC-S1} distribution, in events with the time sequence S1-SEC-S2.

time sequence S1-SEC-S2. We selected the pulses with the same criteria described in Sec. 3. In Fig. 8, we show the SEC charge *vs.* the time difference Δt_{SEC-S1} distribution. We notice that the events are evenly distributed in time and with a SEC charge consistent with single electrons (~ 25 PE). We, therefore, called them *S1-liquid*. The number of events observed in the various categories during the data-taking, and for $\Delta t_{S2-S1} < 50\mu s$, is shown in Tab. 1. While it could be argued that the occurrence of single electrons between S1 and S2 or following an S2 is of random nature, the much larger number of events observed in the

categories S2-liquid compared to S1-liquid, supports the hypothesis that at least the S2-liquid events are indeed correlated with the S1-S2 signals.

To further investigate the hypothesis linking S-liquid events to contaminants, we analysed a set of data taken in a period of five days in July 2015, when the getter was turned off for maintenance. During this period, we expect, as described in [1], an increase of contaminants and, therefore, of S-liquid events. This is indeed observed, as the fraction of S-liquid events increased to $(10.8 \pm 0.7)\%$ from $(8.00 \pm 0.05)\%$, as reported in Tab. 1 for the standard data-taking period. This $\sim 35\%$ increase of S-liquid fraction suggests that at least part of these events are due to the photoelectric extraction from contaminants that are normally trapped by the getter. The rest of them can possibly be due to photoelectric effect on impurities not trapped by the getter or meta-stable states of argon, for which further investigation is needed.

The possibility that single electrons are remnants from the previous event instead of originating from photoelectric effect in the same event was tested by looking at correlations with the preceding events. The time difference distribution between an S1-liquid or an S2-liquid event with any previous event in a time window of 10s did not display any significant time correlation.

The hypothesis of photoelectric extraction in the liquid was also suggested by other investigators in relation to xenon detectors [10, 25, 26]. For instance, in Ref. [10], the authors claim the photo-ionization of a *yet undetermined contaminant species in the liquid xenon* as a possible origin of isolated electrons.

6. Conclusion

We observed several categories of single isolated electrons in association with standard scintillation-ionization signals in the DarkSide-50 LAr TPC. The most abundant one includes S2-echo events, which are low-charge S2-like pulses occurring after one maximum drift time from the previous S2 signal. These signals are induced by scintillation light photo-extracting electrons from the cathode. Given the limited data-acquisition time window, only S2-echoes produced in events with an interaction occurring in the upper ~ 5 cm of the TPC can be detected. Another category, not affected by the limited data-acquisition time window, includes S1-echo events, which contain low-charge pulses occurring one maximum drift time after S1. The probability of such a processes is linked to the photo-ionization probability of the DS-50 cathode, which is made of fused silica and coated with ITO and TPB. We measured its photoelectric extraction probability at wavelengths of 128 nm to be of the order of 0.1%, most probably dominated by the effect on the TPB. Despite the small probability, the number of events with echoes turns out to be about twice the standard two-pulse S1-S2 events, used for WIMP dark matter searches, due to the large number of photons associated with the S2 pulses. Having a definite time delay from S1 and S2 pulses, the echo signals can easily be tagged and therefore do not hinder the dark matter searches.

We also observed events possibly related to interactions of photons in the liquid, S-liquid. Indeed, 128 nm radiation can interact with electro-negative impurities or meta-stable anions along its path, inducing photo-ionization processes in the liquid. We also investigated their relative number in the period of maintenance of DS-50, when

the getter of the purification system was offline and we found that the rate of S-liquid events increased by 35%. This rate increase suggests a relationship between S-liquid signals and impurities in the liquid, that may be further investigated by future work.

Acknowledgements

The DarkSide Collaboration offers its profound gratitude to the LNGS and its staff for their invaluable technical and logistical support. We also thank the Fermilab Particle Physics, Scientific, and Core Computing Divisions. Construction and operation of the DarkSide-50 detector was supported by the U.S. National Science Foundation (NSF) (Grants No. PHY-0919363, No. PHY-1004072, No. PHY-1004054, No. PHY-1242585, No. PHY-1314483, No. PHY-1314501, No. PHY-1314507, No. PHY-1352795, No. PHY-1622415, and associated collaborative grants No. PHY-1211308 and No. PHY-1455351), the Italian Istituto Nazionale di Fisica Nucleare, the U.S. Department of Energy (Contracts No. DE-FG02-91ER40671, No. DEAC02-07CH11359, and No. DE-AC05-76RL01830), the Polish NCN (Grant No. UMO-2014/15/B/ST2/02561) and the Foundation for Polish Science (Grant No. Team2016-2/17). We also acknowledge financial support from the French Institut National de Physique Nucléaire et de Physique des Particules (IN2P3) and the UnivEarthS LabEx program (Grants No. ANR-10-LABX-0023 and No. ANR-18-IDEX-0001), from the São Paulo Research Foundation (FAPESP) (Grant No. 2016/09084-0), from the Interdisciplinary Scientific and Educational School of Moscow University “Fundamental and Applied Space Research”, and from IRAP AstroCeNT funded by FNP from ERDF. Isotopes used in this research were

supplied by the United States Department of Energy Office of Science by the Isotope Program in the Office of Nuclear Physics.

References

- [1] P. Agnes et al. (The DarkSide Collaboration), *Phys. Rev. Lett.* **121**, 081307 (2018).
- [2] P. Agnes et al. (The DarkSide Collaboration), *Phys. Rev. Lett.* **121**, 111303 (2018).
- [3] C. E. Aalseth et al. (The DarkSide Collaboration), *Eur. Phys. J. Plus* **133**, 131 (2018).
- [4] P. Agnes et al., *Nucl. Instrum. Meth. A* **904**, 23 (2018).
- [5] M. G. Boulay and A. Hime, *Astropart. Phys.* **25**, 179 (2006).
- [6] A. Hitachi et al., *Phys. Rev. B* **27**, 5279 (1983).
- [7] P. Agnes et al. (The DarkSide Collaboration), *Phys. Rev. D* **98**, 102006 (2018).
- [8] D. Akimov et al., *Journal of Instrumentation* **11**, C03007 (2016).
- [9] E. Aprile et al., *Journal of Physics G: Nuclear and Particle Physics* **41**, 035201 (2014).
- [10] B. Edwards et al., *Astroparticle Physics* **30**, 54 (2008).
- [11] E. Santos et al., *JHEP* **12**, 115 (2011).
- [12] P. Sorensen, :arXiv:1702.04805 (2017).
- [13] P. Sorensen and K. Kamdin, *JINST* **13**, P02032 (2018).
- [14] J. Angle et al., *Phys. Rev. Lett.* **107**, 051301 (2011).
- [15] E. Aprile et al., *Phys. Rev. Lett.* **123**, 251801 (2019).
- [16] E. Santos et al., *Journal of High Energy Physics* **2011**, 115 (2011).
- [17] D. Acosta-Kane et al., *Nucl. Inst. Meth. A* **587**, 46 (2008).
- [18] J. Xu et al., *Astropart. Phys.* **66**, 53 (2015).
- [19] A. Bondar et al., *JINST* **4**, P09013 (2009).
- [20] P. Agnes et al. (The DarkSide Collaboration), *JINST* **12**, P12011 (2017).
- [21] P. Agnes et al. (The DarkSide Collaboration), *Phys. Lett. B* **743**, 456 (2015).
- [22] R. Acciarri et al. (The WArP Collaboration), *JINST* **5**, P05003 (2010).
- [23] P. Agnes et al., *JINST* **12**, P10015 (2017).
- [24] C. Benson, G. Orebi Gann, and V. Gehman, *Eur. Phys. J. C* **78**, 329 (2018).
- [25] D. Akerib et al., *Phys. Rev. D* **102**, 092004 (2020).
- [26] E. Aprile et al., *J. Phys. G* **41**, 035201 (2014).